Progress In Electromagnetics Research B, Vol. 9, 249–262, 2008

OVERVIEW OF RCS EXTRAPOLATION TECHNIQUES TO AIRCRAFT TARGETS

N. J. Li, C. F. Hu, L. X. Zhang, and J. D. Xu

UAV Specialty Technique Key National Laboratory
Northwestern Polytechnic University
Xi'an, Shaanxi 710072, China

Abstract—In order to meet the approximate plane-wave irradiation condition, adequate large field or compact range system is needed for RCS measurement of large aircraft targets. However, an outside testing field site or a compact range system is very expensive, so some kinds of RCS extrapolation methods based on near-distance testing have been presented. In this overview, two categories of extrapolating technique are summed up, which are based on Huygens Equivalent Reradiating Source (HERS) and Inverse Synthetic Aperture Imaging (ISAI) respectively. Each method is fully elaborated. The comparison and analysis of these extrapolating techniques are discussed in detail.

1. INTRODUCTION

RCS measurement is of great significance to the research of stealth target and its scattering characteristics. Generally it needs huge testing field or complex expensive compact range system [1, 2]. However, an outside test field site or a compact range system is very expensive. In order to overcome this problem, a variety of near-field test method to extrapolate RCS came into being [3–13]. In this overview, two categories are summed up from the existing extrapolating techniques, the one is based on Huygens Equivalent Reradiating Source (HERS), and the other is based on inverse synthetic aperture imaging (ISAI).

The near-distance RCS measurement system is identical to far-field, but the distance is much shorter, so the testing distance can easily be met and the RCS of targets are obtained by extrapolating techniques. In this paper, several extrapolating technologies are described in detail, and the precision, effective angle domain and applicability are discussed.

Table 1 lists a number of scaled aircraft models; the height of fuselage is less than 1/7 of its length. So they can easily meet the far field RCS testing requirements in vertical direction (Table 2 shows the allowed maximum height of a target at different frequencies) according far-field condition. Therefore, for the near-field RCS measurement, field distribution in the target range can be regarded approximately as a cylindrical wave. Based on above assumption, two kinds of extrapolating technique can be derived.

Table 1. The height and length of some scaled models.

Model	**Global Hawk**	**B2**	**F22**	**Dark Star**
length/(m)	1.90	2.00	2.50	3.30
height/(m)	0.15	0.12	0.35	0.20
Height/length	0.079	0.061	0.14	0.064

Table 2. The maximum height allowed for targets at different frequencies.

Test Distance $R = 20\,\mathrm{m}$					
Frequency/GHz	1	2	5	10	30
maximum height/m	1.73	1.22	0.77	0.55	0.35

In general, the extrapolation of far field RCS from near field data requires a full set of bistatic scattering measurements. La Haie developed a new near field-to-far field transformations (NFFFT) for predicting the far-field RCS of targets from monostatic near-field measurements [5, 6]. His techniques use approximations and/or supporting information to overcome the need for bistatic near-field measurement [7, 8].

For predicting far-field RCS, three new methods named Huygens arithmetic, Hankel arithmetic and NFFFT are realized in this paper, Huygens arithmetic is based on HERS, the Hankel arithmetic is based on ISAI, NFFFT is another arithmetic based on ISAI, which can be used in stepped-frequency measurement system.

In the following, a uniform and innovative view is set up to understand all the extrapolating techniques.

2. METHODS OF RCS EXTRAPOLATION FROM NEAR-FIELD TO FAR-FIELD

2.1. The Relation between Near-field and Far-field Based on Imaging

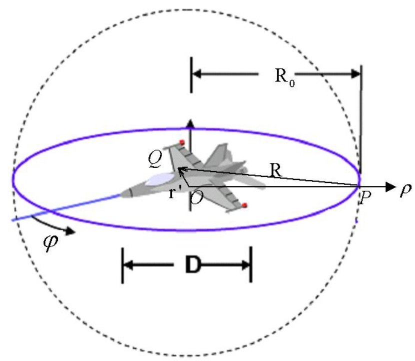

Figure 1. Near-field RCS measurement.

As shown in Figure 1, P point is the position of radar, O point is the centre of rotator, Q point is a selected point on target randomly. Based on the assumption that the reflectivity distribution of target is irrelative to distance of measurement, the basic 2-D imaging formula can be expressed as following:

$$S_r(t) = \int_V g(\boldsymbol{r'}) S_t\left(t - \frac{2R}{c}\right) d\boldsymbol{r'} \tag{1}$$

In above equation, $\boldsymbol{r'}$ is any selected point position vector on the target, R is the range from radar to target, $g(\boldsymbol{r'})$ is the reflectivity distributing function within the target, which can be derived by 2-D Fourier transformation, as follow:

$$g(\boldsymbol{r'}) = \int_V S_r(t) S_t^*\left(t - \frac{2R}{c}\right) e^{-j\boldsymbol{K}\cdot\boldsymbol{r'}} d\boldsymbol{K} \tag{2}$$

As we know, Green function in free space can be expressed as $G(k, \boldsymbol{R}_0) = e^{-jk|\boldsymbol{R}_0 - \boldsymbol{r'}|}/4\pi|\boldsymbol{R}_0 - \boldsymbol{r'}|$. Similarly, the every point of imaging can be regarded as reradiating source, thus the new Green function is derived as $G(k, \boldsymbol{R}_0) = e^{-j2k|\boldsymbol{R}_0 - \boldsymbol{r'}|}/(4\pi|\boldsymbol{R}_0 - \boldsymbol{r'}|)^2$. The scattering field collected by radar in near-field can be expressed as following

$$E_s^N(k, \boldsymbol{R}_0) = \frac{1}{(4\pi)^2} \int\limits_V g(\boldsymbol{r'}) e^{-j2k|\boldsymbol{R}_0 - \boldsymbol{r'}|} / |\boldsymbol{R}_0 - \boldsymbol{r'}|^2 d\boldsymbol{r'} \tag{3}$$

where k is the wave number, $\boldsymbol{R}_0$ is the position vector of radar observation point.

The echo signal of radar in far-field is:

$$\begin{aligned} E_s^F(k, \boldsymbol{R}) &= \frac{1}{(4\pi)^2} \int\limits_V \frac{g(\boldsymbol{r'})}{|\boldsymbol{R} - \boldsymbol{r'}|^2} e^{-j2k|\boldsymbol{R} - \boldsymbol{r'}|} d\boldsymbol{r'} \\ &\approx \frac{e^{-j2k|\boldsymbol{R}|}}{(4\pi|\boldsymbol{R}|)^2} \int\limits_V g(\boldsymbol{r'}) e^{j2k\boldsymbol{r'} \cdot \hat{\mathbf{R}}} d\boldsymbol{r'} \end{aligned} \tag{4}$$

From the relation between Equation (3) and Equation (4), the distance factor $|\boldsymbol{R}_0 - \boldsymbol{r'}|$ in Equation (3) can be reduced approximately to three forms according to different near distance, so we can derive three arithmetic.

2.2. Huygens Arithmetic-Extrapolating Technique Based on HERS

If $R_0 \gg r'_{\max}$, $r'_{\max}$ is the maximum size of target, the denominator $|\boldsymbol{R}_0 - \boldsymbol{r'}|^2$ in Equation (3) can be approximated as $|\boldsymbol{R}_0|^2$, thus, the near-field of target is treated as a new second radiating source, the second radiating pattern can be calculated from Equation (3), as following:

$$\begin{aligned} E_s^N(k, \boldsymbol{R}_0) &= \frac{1}{(4\pi)^2} \int\limits_V \frac{g(\boldsymbol{r'})}{|\boldsymbol{R}_0 - \boldsymbol{r'}|^2} \cdot e^{-j2k|\boldsymbol{R}_0 - \boldsymbol{r'}|} d\boldsymbol{r'} \\ &\approx \frac{1}{(4\pi|\boldsymbol{R}_0|)^2} \int\limits_V g(\boldsymbol{r'}) \cdot e^{-j2k|\boldsymbol{R}_0 - \boldsymbol{r'}|} d\boldsymbol{r'} \\ &\approx C \cdot g(\boldsymbol{r'}) * e^{-j2k\boldsymbol{R}_0} \end{aligned} \tag{5}$$

where $C = 1/(4\pi|\boldsymbol{R}_0|)^2$, C is a constant which can be ignored, $*$ is convolution operator. By replacing convolution by Fourier transform [16], we can get:

$$g(\boldsymbol{r'}) \approx \mathbb{F}^{-1} \left\{ \mathbb{F}\left[E_s^N(k, \boldsymbol{R}_0)\right] / \mathbb{F}\left(e^{-j2k\boldsymbol{R}_0}\right) \right\} \tag{6}$$

So the far field of target is derived as:

$$E_s^F(k,\boldsymbol{R}) \approx \frac{1}{|\boldsymbol{R}|^2}\int\limits_V g(\boldsymbol{r'})\cdot e^{-j2k|\boldsymbol{R}-\boldsymbol{r'}|}d\boldsymbol{r'} \approx g(\boldsymbol{r'}) * e^{-j2k\boldsymbol{R}} \tag{7}$$

Rewrite Equation (6) and Equation (7), the relation between near-field and far-field can be established as following:

$$E_s^F(k,\boldsymbol{R}) \approx \mathbb{F}^{-1}\left\{\mathbb{F}\left[E_s^N(k,\boldsymbol{R}_0)\right]\cdot\mathbb{F}\left(e^{-j2k\boldsymbol{R}}\right)/\mathbb{F}\left(e^{-j2k\boldsymbol{R}_0}\right)\right\} \tag{8}$$

2.3. Hankel Arithmetic-Extrapolating Technique Based on ISAI

Equation (3) can be coordinated to the format including Green Function of 2-D free space, as follows:

$$\begin{aligned} E_s^N(k,\boldsymbol{R}_0) &= \int\limits_V \frac{\sqrt{2k}\cdot g(\boldsymbol{r'})}{|\boldsymbol{R}_0-\boldsymbol{r'}|^{3/2}}\cdot\frac{e^{-j2k|\boldsymbol{R}_0-\boldsymbol{r'}|}}{\sqrt{2k|\boldsymbol{R}_0-\boldsymbol{r'}|}}d\boldsymbol{r'} \\ &\approx \int\limits_V \frac{\sqrt{2k}\cdot g(\boldsymbol{r'})}{|\boldsymbol{R}_0-\boldsymbol{r'}|^{3/2}}\cdot C'\cdot H_0^{(2)}\left(2k\left|\boldsymbol{R}_0-\boldsymbol{r'}\right|\right)d\boldsymbol{r'} \end{aligned} \tag{9}$$

In Equation (9), the error can be analyzed by assuming $Ratio = \frac{e^{-j2kR|}}{\sqrt{2kR}}/H_0^{(2)}(2kR)$, Let $k = 10$ (frequency is 0.5 GHz), distance R varies from 1 m to 8 m, The result is listed in Table 3.

Table 3. The approximation error of amplitude and phase.

R /m	1	2	3	4	5	6	7	8
$2kR$	20	40	60	80	100	120	140	160
$\lvert Ratio\rvert$	5.606	5.605	5.605	5.605	5.605	5.605	5.605	5.605
arg($Ratio$) /degree	-45.36	-45.18	-45.12	-45.09	-45.07	-45.06	-45.05	-45.05

The error of amplitude is lower than 0.02% and the error of phase is lower than 0.5°. So Equation (9) has an excellent precision.

In Equation (9), C' is a constant. If $R_0 \gg r'_{\max}$, the denominator $|\boldsymbol{R}_0 - \boldsymbol{r}'_0|$ in Equation (9) can be approximated as $|\boldsymbol{R}_0|$, also named

R_0. According to the Hankel addition theory:

$$H_0^{(2)}\left(2k\left|\boldsymbol{R}_0-\boldsymbol{r'}\right|\right)=\sum_{n=-\infty}^{\infty}H_n^{(2)}(2kR_0)J_n(2kr')e^{jn(\varphi_0-\varphi')} \tag{10}$$

Replacing Equation (10) to Equation (9), and ignoring the constant C', a series is derived as following:

$$E_s^N(k,\boldsymbol{R}_0)\approx\frac{2k}{R_0^{3/2}}\sum_{n=-\infty}^{\infty}H_n^{(2)}(2kR_0)e^{jn\varphi_0}\int\limits_V g(\boldsymbol{r'})J_n(2kr')e^{-jn\varphi'}d\boldsymbol{r'} \tag{11}$$

Note $\int\limits_V g(\boldsymbol{r'})J_n(2kr')e^{-jn\varphi'}d\boldsymbol{r'}=S_n^{2k}$, this is the generalized Fourier series of target image, which belongs to inherence scattering characteristic, and it is irrelative to measurement distance. So Equation (11) can be changed as:

$$E_s^N(k,\mathbf{R}_0)\approx\frac{2k}{R_0^{3/2}}\sum_{n=-\infty}^{\infty}S_n^{2k}H_n^{(2)}(2kR_0)e^{jn\varphi_0} \tag{12}$$

According to the large argument approximation theory in Hankel function, Equation (12) is turned as:

$$E_s^F(k,\boldsymbol{R})\approx\frac{1}{R^2}\sqrt{\frac{4k}{\pi}}e^{j\left(2-kR+\frac{\pi}{4}\right)}\sum_{n=-\infty}^{\infty}S_n^{2k}e^{jn\left(\varphi+\frac{\pi}{2}\right)} \tag{13}$$

Connect Equation (12) and Equation (13), the following can be derived:

$$\begin{aligned}E_s^F(k,\boldsymbol{R})&\approx\int E_s^N(k,\boldsymbol{R}_0)\sum_{n=-\infty}^{\infty}\frac{j^ne^{jn(\varphi-\varphi_0)}}{H_n^{(2)}(2kR_0)}d\varphi_0\\&=E_s^N(k,\varphi_0)*\sum_{n=-\infty}^{\infty}\frac{j^ne^{jn(\varphi_0)}}{H_n^{(2)}(2kR_0)}\end{aligned} \tag{14}$$

In fact, the series in Equation (14) must be truncated, generally $|n|\leq N_0$, $N_0\geq int(2kD)$, where D is the minimum radius enclosing the target.

2.4. NFFFT-Another Extrapolating Technique Based on ISAI

If the testing distance is much nearer, the assumption $R_0 \gg r'_{\max}$ can not be met, a more precise technique is needed [14]. Rewrite Equation (3), as following:

$$E_s^N(k, \boldsymbol{R}_0) = \int_V g(\boldsymbol{r'}) \cdot \frac{e^{-j2k|\boldsymbol{R}_0 - \boldsymbol{r'}|}}{|\boldsymbol{R}_0 - \boldsymbol{r'}|^2} d\boldsymbol{r'} \tag{15}$$

Do partial derivative of k to Equation (15):

$$\begin{aligned} \frac{\partial E_s^N(k, \boldsymbol{R}_0)}{\partial k} &= \int_V -j2 \cdot g(\boldsymbol{r'}) \cdot \frac{e^{-j2k|\boldsymbol{R}_0 - \boldsymbol{r'}|}}{|\boldsymbol{R}_0 - \boldsymbol{r'}|} d\boldsymbol{r'} \\ &\approx \int_V -j2 \cdot \frac{g(\boldsymbol{r'})}{|\boldsymbol{R}_0 - \boldsymbol{r'}|^{1/2}} \cdot c' H_0^{(2)}\left(2k\left|\boldsymbol{R}_0 - \boldsymbol{r'}\right|\right) d\boldsymbol{r'} \end{aligned} \tag{16}$$

Note $-\frac{1}{j2} \cdot \frac{\partial E_s^N(k, \boldsymbol{R}_0)}{\partial k} \triangleq U_s^N$, if we use stepped-frequency RCS measurement system, U_s^N can be easily obtained by Fourier Transform technique as [18–21]:

$$U_s^N(k, \boldsymbol{R}_0) = \frac{1}{2\pi} \int 2R \left[\int E_s^N(k, R_0) e^{j2kR_0} dk \right] e^{-j2kR} dR \tag{17}$$

Ignore the constant c', Equation (16) is changed as:

$$U_s^N \approx \frac{1}{R_0^{1/2}} \int_V -j2 \cdot g(\boldsymbol{r'}) \cdot H_0^{(2)}\left(2k\left|\boldsymbol{R}_0 - \boldsymbol{r'}\right|\right) d\boldsymbol{r'} \tag{18}$$

In Equation (17), U_s^N is derived from near field $E_s^N(k', R_0)$ by inverse Fourier transform, and after multiplying distance factor $2R$, Fourier transform is used once more. In fact, if R is replaced by $R^{3/2}$, as following:

$$U_s^N(k, \boldsymbol{R}_0) = \frac{1}{2\pi} \int 2R^{3/2} \left[\int E_s^N(k, R_0) e^{j2kR_0} dk \right] e^{-j2kR} dR \tag{19}$$

Thus, $1/|\boldsymbol{R}_0 - \boldsymbol{r'}|^{1/2}$ is approximated as $1/\boldsymbol{R}_0^{1/2}$ by moving from the integral with much less error in Equation (18) (shown in Figure 2).

According to the Hankel addition theory, the far-field can be derived from the near-filed as following:

$$\begin{aligned} E_s^F(k,\boldsymbol{R}) &\approx \sqrt{\frac{R_0}{R}}\int U_s^N(k,\boldsymbol{R}_0)\sum_{n=-\infty}^{\infty}\frac{j^n e^{jn(\varphi-\varphi_0)}}{H_0^{(2)}(2kR_0)}d\varphi_0 \\ &= U_s^N(k,\varphi_0) * \sqrt{\frac{R_0}{R}}\sum_{n=-\infty}^{\infty}\frac{j^n e^{jn(\varphi_0)}}{H_0^{(2)}(2kR_0)} \end{aligned} \tag{20}$$

Similar to Equation (14), Equation (20) must be truncated, generally $|n| \leq N_0$, $N_0 \geq kD + 10$, where D is the minimum radius enclosing the target.

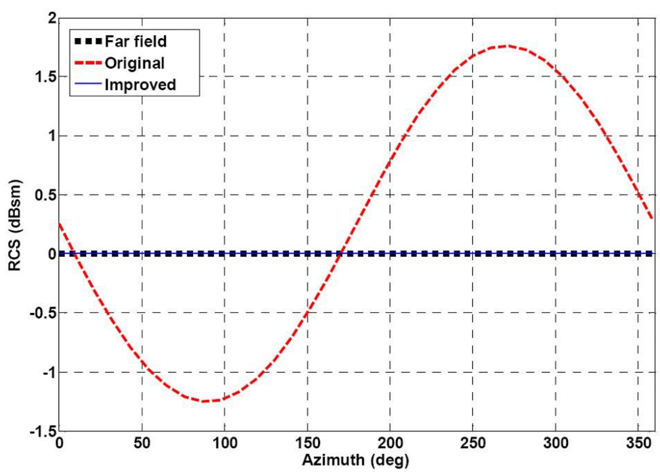

Figure 2. Much less error is gained by replacing R with $R^{3/2}$ (the dash line turns solid line).

The above two arithmetic are based on inverse synthesized aperture imaging theory, despite their theoretical underpinnings. However, they do not explicitly require image formation as part of their implementation, so they are the most computationally efficient.

3. SIMULATION AND EXPERIMENTS

A plate with length 1m, and width 0.3 m, is selected as DUT, frequency is 15 GHz, the distance is 16 m, and the scope of rotator is $-7.5° \sim 7.5°$, where the step is $0.1°$, as shown in Figure 3. The simulated result is shown in Figure 4. By extrapolating the near-field with Huygens

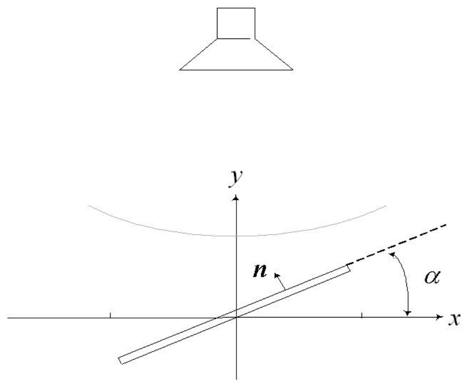

Figure 3. Metal plate rotates by α angle.

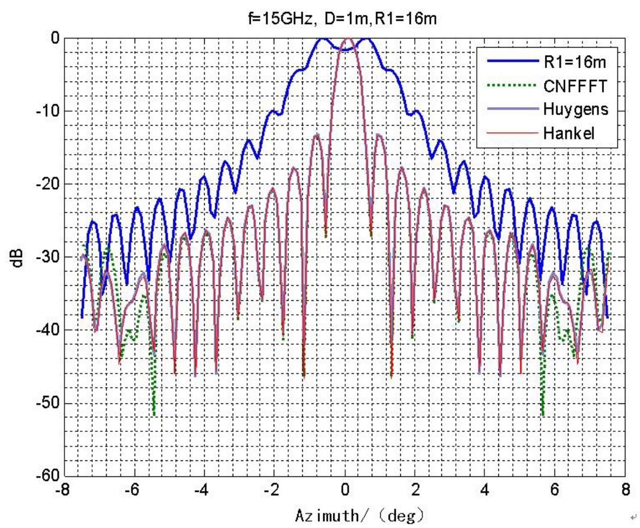

Figure 4. Normalized RCS patterns by extrapolating the near-field with Huygens arithmetic, Hankel arithmetic, NFFFT respectively.

arithmetic, Hankel arithmetic and NFFFT respectively, they can be consistent well, all can correct the bend phase-distribution effectively.

The experiment is designed to make a target with large depth structure, which is made of 9 metal spheres with the same diameter 5 mm, as shown in Figure 5, the maximums size in landscape orientation and in depth is 1 m. The measurement frequency is 15 GHz,

Figure 5. A target with large depth structure.

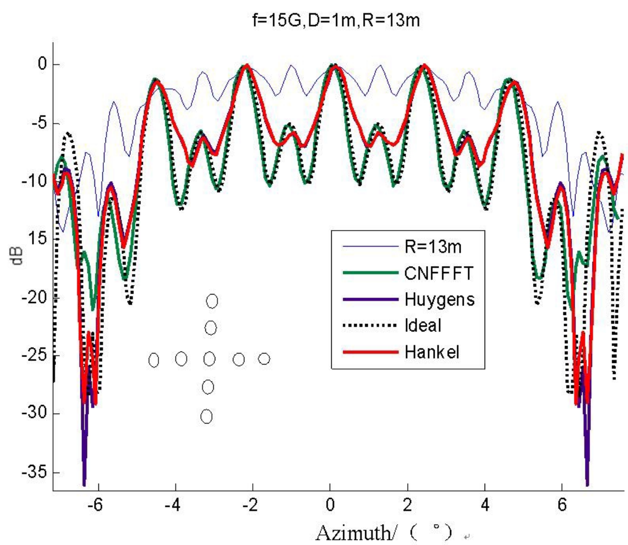

Figure 6. Normalized RCS patterns by extrapolating the near-field with Huygens arithmetic, Hankel arithmetic and NFFFT Respectively.

the distance is 13 m, and the scope of rotator is $-7.5^\circ \sim 7.5^\circ$, where the step is 0.1°. The experimental result is shown in Figure 6. NFFFT holds the best precision, its extrapolating results are very consistent with theoretical value within $-5^\circ \sim 5^\circ$, the two small sides are not consistent with theoretical value because the arithmetic has limited angle scope. Huygens arithmetic, Hankel arithmetic can hold little error in high level, but more error occurs in lower level. The error caused by the distance factor is approximated too serious when extracted from the integral in Equation (5) and Equation (11).

The results in simulation and experiment show that three extrapolating techniques can extrapolate the true RCS effectively, NFFFT technique gets the best precision especially for near-field measurement. The base of the extrapolating technique is scattering center model, which is suit for most of aircraft targets [22–26]. In addition, the existing RCS measurement systems generally are bistatic, the monostatic RCS can be gained according to the bistatic and monostatic RCS equivalence principle [27]. Also, this principle is based on Scattering Center model [28–31]. So the extrapolating techniques can be applied to general RCS measurement systems.

4. CONCLUSIONS

As above, three extrapolating techniques are described. They all can be applied to whole circle angle scope, so the whole circle RCS can be gained. Huygens extrapolation technique requires farther distance to obtain lower magnitude error. Hankel extrapolation techniques can apply to less distance by amending part error. NFFFT is the most precision for no magnitude approximation, and it can be used at very near distance.

During the process of real target rotating and imaging, large angle scope leads the scattering centers migrate. In fact, extrapolating techniques based on ISAR imaging theory are also applied to small rotator angle scope mostly. The whole circle RCS can be depicted by connecting every sect of small rotator angle scope.

ACKNOWLEDGMENT

I am grateful to Prof. W. L. Wang, UAV Specialty Technique Key Laboratory of National Technology, Northwestern Polytechnic University, for his helpful advice. Any errors are of course my responsibility.

REFERENCES

1. Knott, E. F., et al., *Radar Cross Section*, Artech House, Inc., Dedham, MA, 2004.
2. Falconer, D. G., "Extrapolation of near-field RCS measurements to the far zone," *IEEE Trans. Antennas Propagation*, Vol. 36, No. 6, 822–829, 1988.

3. Birtcher, C. R., C. A. Balanis, and V. J. Vokurka, "RCS measurements, transformations and comparisons under cylindrical and plane wave illumination," *IEEE Trans. Antennas Propagation*, Vol. 42, No. 3, 329–333, 1994.
4. Odendaal, J. W. and J. Joubert, "Radar cross section measurements using near-field radar imaging," *IEEE Trans. on Instrumentation and Measurement*, Vol. 45, No. 6, 948–954, 1996.
5. LaHaie, I. J., "Overview of an image-based technique for predicting far field radar cross-section from near field measurements," *IEEE Ant. Prop. Mag.*, Vol. 45, No. 6, 159–169, 2003.
6. LaHaie, I. J., "An improved version of the circular near field-to-far field transformation (CNFFFT)," *Proceedings of the 27th Annual Meeting of the Antenna Measurement Techniques Association (AMTA'05)*, 196–201, Newport, RI, 2005.
7. Gelius, L. J., "Electromagnetic scattering approximations revisited," *Progress In Electromagnetics Research*, PIER 76, 75–94, 2007.
8. Leou, J. L. and H. J. Li, "Evaluation of bistatic far-field quantities from near-field measurements," *Progress In Electromagnetics Research*, PIER 25, 167–188, 2000.
9. Melin, J., "Measuring radar cross section at short distances," *IEEE Trans. Antennas Propagation*, Vol. 35, No. 6, 991–996, 1987.
10. Broq Uetas, A., J. Palau, and L. Jofre, "Spherical wave near-field imaging and radar cross section measurement," *IEEE Trans. on Antennas and Propagation*, Vol. 46, No. 5, 730–735, 1998.
11. Cown, B. J. and C. E. Ryan, "Near-field scattering measurement for determining complex target RCS," *IEEE Trans. on Antennas and Propagation*, Vol. 37, No. 5, 576–585, 1989.
12. Inasawa, Y., I. Chiba, and S. Makino, "Prediction of far-field bistatic scattering cross section using spherical, cylindrical and planar scanned near-field data," *Proc. 11th conf. Antennas and Propagation*, 599–602, 2001.
13. Chang, D. C., M. C. Tzay, and R. C. Chung, "Far field RCS prediction by near field RCS measurement," *Proceedings of APMC*, 2001.
14. Jarem, J. M., "Validation and numerical convergence of the Hankel-Bessel and Mathieu rigorous coupled wave analysis algorithms for radically and azimuthally inhomogeneous, elliptical, cylindrical systems," *Progress In Electromagnetics Research*, PIER 36, 153–177, 2002.

15. Hu, W., H. Sun, and X. Lv, "Research on RCS measurement under non-far field condition," *IEEE Trans. Antennas Propagation*, Vol. 51, No. 3, 392–395, 2003.
16. Zhang, H. Y., "RCS calculation, transformations and comparisons under spherical and plane wave illumination," *IEEE Trans. Antennas Propagation*, Vol. 43, No. 12, 1918–1921, 1995.
17. Xin, Y. F. and P.-L. Rui, "Adaptively accelerated gmres fast fourier transform method for electromagnetic scattering," *Progress In Electromagnetics Research*, PIER 81, 303–314, 2008.
18. Weedon, W. H., "A step-frequency radar imaging system for microwave nondestructive evaluation," *Progress In Electromagnetics Research*, PIER 28, 121–146, 2000.
19. Hu, C.-F., J.-D. Xu, N. Li, and L. Zhang, "Indoor accurate RCS measurement technique on UHF band," *Progress In Electromagnetics Research*, PIER 81, 279–289, 2008.
20. Li, H.-J., H.-C. Lin, C.-C. Chen, T.-Y. Liu, and Z.-Y. Lane, "Determination of propagation mechanisms using wideband measurement techniques," *Progress In Electromagnetics Research*, PIER 20, 283–299, 1998.
21. Weedon, W. H., W. C. Chew, and P. E. Mayes, "A step-frequency radar imaging system for microwave nondestructive evaluation," *Progress In Electromagnetics Research*, PIER 28, 121–146, 2000.
22. Gelius, L. J., "Electromagnetic scattering approximations revisited," *Progress In Electromagnetics Research*, PIER 76, 75–94, 2007.
23. Mouysset, V., P. A. Mazet, and P. Borderies, "A new approach to evaluate accurately and efficiently electromagnetic fields outside a bounded zone with time-domain volumic methods," *Journal of Electromagnetic Waves and Applications*, Vol. 20, No. 6, 803–817, 2006.
24. Rui, P.-L. and R.-S. Chen, "Implicitly restarted gmres fast Fourier transform method for electromagnetic scattering," *Journal of Electromagnetic Waves and Applications*, Vol. 21, No. 7, 973–986, 2007.
25. Li, Y.-L., J.-Y. Huang, M.-J. Wang, and J. Zhang, "Scattering field for the ellipsoidal targets irradiated by an electromagnetic wave with arbitrary polarizing and propagating direction," *Progress In Electromagnetics Research Letters*, Vol. 1, 221–235, 2008.
26. Li, X.-F., Y.-J. Xie, and R. Yang, "High-frequency method analysis on scattering from homogenous dielectric objects with

electrically large size in half space," *Progress In Electromagnetics Research B*, Vol. 1, 177–188, 2008.

27. Falconer, D. G., "Near-field statement of monostatic-bistatic theorem," *Abstracts 1988 URSI Nat. Radio Science Meeting*, Jan. 1988.
28. Lee, K.-C. and J.-S. Ou, "Radar target recognition by using linear discriminant algorithm on angular-diversity RCS," *Journal of Electromagnetic Waves and Applications*, Vol. 21, No. 14, 2033–2048, 2007.
29. Li, Y.-L., J.-Y. Huang, M.-J. Wang, and S.-H. Gong, "The scattering cross section for a target irradiated by time-varying electromagnetic waves," *Journal of Electromagnetic Waves and Applications*, Vol. 21, No. 9, 1265–1271, 2007.
30. Li, Y.-L., J.-Y. Huang, and M.-J. Wang, "Scattering cross section for airborne and its application," *Journal of Electromagnetic Waves and Applications*, Vol. 21, No. 15, 2341–2349, 2007.
31. D'Agostino, F., F. Ferrara, C. Gennarelli, R. Guerriero, and M. Migliozzi, "Near-field-far-field transformation technique with helicoidal scanning for elongated antennas," *Progress In Electromagnetics Research B*, Vol. 4, 249–261, 2008.